BULLETIN OF THE POLISH ACADEMY OF SCIENCES
TECHNICAL SCIENCES, Vol. 70(1), 2022, Article number: e140099
DOI: 10.24425/bpasts.2022.140099

Influence of the stator current reconstruction method on direct torque control of induction motor drive in current sensor postfault operation

Michal ADAMCZYK*, and Teresa ORLOWSKA-KOWALSKA

Department of Electrical Machines, Drives and Measurements, Wroclaw University of Science and Technology,
Wybrzeże Wyspiańskiego 27, 50-370 Wrocław, Poland

Abstract. Modern induction motor (IM) drives with a higher degree of safety should be equipped with fault-tolerant control (FTC) solutions. Current sensor (CS) failures constitute a serious problem in systems using vector control strategies for IMs because these methods require state variable reconstruction, which is usually based on the IM mathematical model and stator current measurement. This article presents an analysis of the operation of the direct torque control (DTC) for IM drive with stator current reconstruction after CSs damage. These reconstructed currents are used for the stator flux and electromagnetic torque estimation in the DTC with space-vector-modulation (SVM) drive. In this research complete damage to both stator CSs is assumed, and the stator current vector components in the postfault mode are reconstructed based on the DC link voltage of the voltage source inverter (VSI) and angular rotor speed measurements using the so-called virtual current sensor (VCS), based on the IM mathematical model. Numerous simulation and experimental tests results illustrate the behavior of the drive system in different operating conditions. The correctness of the stator current reconstruction is also analyzed taking into account motor parameter uncertainties, especially stator and rotor resistances, which usually are the main parameters that determine the proper operation of the stator flux and torque estimation in the DTC control structure.

Key words: current sensor faults; induction motor drive; direct torque control; current estimator; fault-tolerant control.

1. INTRODUCTION

For over 30 years, there has been a growing interest in adjustable-speed drives (ASD) with AC motors, including induction motors (IMs) due to their simple structure, and thus low failure rate, among others. However, due to the operating conditions or random events, various types of damage may occur in IM drive systems. Failures may be related to the motor [1], voltage inverter [2–4] (e.g. damage to the IGBT transistors [5,6]), but also to measuring equipment [7–11], such as resolvers [12], encoders [13–17], sensors for measuring currents and voltages [8, 14, 15, 18].

In view of the above, in recent years systems with an increased level of safety have become more and more popular. Currently, fault-tolerant control (FTC) solutions are presented in the literature, and their concept has been thoroughly described in [19–21], among others. As presented there, we can distinguish hardware and software redundancy in ASD.

The first strategy assumes redundancy of measuring, control, or executive devices [21], which sometimes are very expensive. It is much more attractive in terms of maintaining the overall functionality of the system but is associated with high costs. To avoid them, a better solution seems to be the second strategy, i.e. software redundancy, in which the main assumption is to design a fault detection system and, in the event of a failure, to isolate it and use specific algorithmic solutions for fault compensation.

Current sensor (CS) failures are one of the most frequent in the case of measuring equipment [22–24]. LEM-type transducers are most often used to measure the current. Among the CS faults presented in [25] together with the mathematical models, some can be compensated before the startup or during the operation of the system [26], and some limit the operation of the system to a significant extent. The first group includes measurement offsets, gain errors, or measurement noise [7] and [27], while the second group includes saturation, interruption, or complete loss of the signal.

Accurate information about the current signal is necessary in IM drives for the correct estimation of difficult-to-measure state variables, such as rotor flux in the case of the field-oriented control (FOC) methods and stator flux or electromagnetic torque for the direct torque control (DTC) methods. Inaccurate current measurement can significantly deteriorate the quality of the drive system operation, while the complete loss of information about the value of the IM phase current prevents the operation of vector control structures and requires the transition to the simplest scalar control [22]. Therefore, current sensor fault-tolerant control (CS–FTC) systems deserve special attention since the loss of information about the stator current of a driving motor is related to the inability to precisely control AC motor drives.

*e-mail: michal.adamczyk@pwr.edu.pl

Manuscript submitted 2021-07-15, revised 2021-12-02, initially accepted for publication 2021-12-06, published in February 2022.

In the known literature, several CS–FTC strategies can be found, depending on the number of damaged CSs and the type of damage. In a situation in which it is possible to measure the stator current in two phases in the ADS, the Clarke transform makes it possible to provide the control structure with this state variable in a stationary coordinate system ($\alpha-\beta$). For this reason, very often in industrial drive systems, the CS is not placed in phase C. One of the CS–FTC solutions proposed in [26] is directed to systems with a sudden signal gain error. The author presented the specific gain function that was used in the measured output signal. Offsets can be reduced before drive start operation when the measured value should be equal to zero. It is worth mentioning that this solution does not require knowledge of the mathematical model of the motor, so this method is insensitive to changes in its parameters.

Another solution that does not use the IM mathematical model, and thus is insensitive to changes in motor parameters, is the appropriate transformation of the coordinate system [28, 29]. In [28] the values of the stator currents in the stationary reference frame, ($\alpha-\beta$), in the FOC control structure are estimated based on their reference values in the synchronously rotating reference frame, ($d-q$). However, the authors present simulation and experimental studies only in the case when one CS remains healthy in the drive system. The application of this method was also proposed in [29] for the direct torque control with space-vector-modulation (DTC-SVM) and additional decoupling of the stator voltage. Moreover, the authors presented the application of the described method in the subway application, and the results obtained by them are compared with those obtained with the method [28] (without voltage decoupling), showing a significant improvement in the quality of the drive system operation on transients.

Methods of stator current reconstruction based on the IM mathematical model are characterized by a much higher quality of work, but unfortunately are susceptible to changes in IM parameters. In the literature, there are solutions addressed to both vector control methods: FOC [30–33] and DTC with switching table (DTC–ST) [24, 34]. In [24] the authors present the flux-linkage observer, implemented in the rotating coordinate system ($d-q$). For the correct estimation of the stator flux and the electromagnetic torque of the IM, it is necessary to measure the angular velocity. As the authors write, this method is very sensitive to changes in IM parameters. A similar solution, using the Luenberger observer, was presented in [34], also for the DTC–ST structure. It should be emphasized that in the case of the published CS–FTC concept regarding the DTC–ST structure with the stator current reconstruction based on the IM mathematical models [24, 34], the authors presented the operation of the system in the postfault mode only for a constant value of the angular velocity or load torque. It is not shown there how the system performs without stator current measurement under other operating conditions, in particular when changing speed and load torque or during reversal operation.

In the literature known to authors, control methods without measuring phase currents in the DTC–SVM structure were presented only in a strategy with an additional DC CS (or a shunt resistor) in the DC link of the voltage source inverter (VSI) [35]. This strategy can also be found in the case of DTC–ST [36] and the FOC structure [37]. However, it is worth mentioning that reconstruction of the stator phase current based on the current in the DC link of VSI entails numerous complications in the implementation of the modulation algorithms [35–37], and often also the necessity to interfere with the IGBT connections [38]. Therefore, this method is used in low-cost systems (with one CS only). Its application in the postfault operation of the classic solutions of ADS (with two-phase CSs) for stator current reconstruction would require an additional sensor in the DC circuit, which is unprofitable.

Thus the main goal of the research presented in this article was to analyze the possibility of application of so-called virtual current sensor (VCS) [31] for the reconstruction of the IM stator phase current in a postfault operation of the DTC–SVM drive system. An analysis of the drive operation in the case of damage of both stator current sensors, required for the stator flux and electromagnetic torque estimation in this control structure, was performed. The stator current vector components in the postfault mode are reconstructed based on measurements of the angular rotor speed and the voltage in the DC link of VSI, according to the VCS algorithm. Simulation tests include also the analysis of the influence of resistance parameters on the proposed stator current reconstruction method applied in DTC structure. Research results presented here illustrate the CSs postfault operation of the analyzed drive for different reference speed values in the whole rated range as well as under load torque changes and during specific transients like slow reversal operation. In addition, the operation of the FTC system is shown also during regenerative brake and regenerating mode, which is not found in the literature. All simulation tests were experimentally verified under the same operating conditions of the drive system.

This article consists of six sections. After the introduction, the mathematical model of the analyzed drive system is presented in Section 2. In this section, the DTC–SVM structure is described except for the IM mathematical model, taking into account the CS postfault control using the proposed stator current estimation method. This method, based on VCS is presented in Section 3. In Section 4, the influence of the stator and rotor resistance to the quality of stator current estimation for different speeds has been presented. Section 5 contains the brief description of the simulation platform and laboratory setup, as well as the simulation and experimental test scenarios. The main part of this section consists in the presentation and analysis of the extensive simulation and experimental results, realized in the same operation conditions of the drive system. The article finishes with concluding remarks.

2. MATHEMATICAL MODEL OF THE DRIVE SYSTEM

2.1. Mathematical model of the induction motor

In this work, the well-known mathematical model of IM, with commonly applied simplifying assumptions [39] is used. It is represented using spatial vectors, in a stationary coordinate system ($\alpha-\beta$), in relative quantities, [p.u.] as follows [40]:

- voltage equations of the stator and rotor windings:

$$T_N \frac{\mathrm{d}}{\mathrm{d}t}\boldsymbol{\Psi}_s = \mathbf{u}_s - r_s \mathbf{i}_s \,, \tag{1}$$

$$T_N \frac{\mathrm{d}}{\mathrm{d}t}\boldsymbol{\Psi}_r = \frac{r_r}{l_r}\left(l_m \mathbf{i}_s - \boldsymbol{\Psi}_r\right) + j\omega_m \boldsymbol{\Psi}_r \,, \tag{2}$$

- flux-current equations:

$$\boldsymbol{\Psi}_s = l_s \mathbf{i}_s + l_m \mathbf{i}_r \,, \tag{3}$$

$$\boldsymbol{\Psi}_r = l_r \mathbf{i}_r + l_m \mathbf{i}_s \,, \tag{4}$$

- equation of motion:

$$T_M \frac{\mathrm{d}}{\mathrm{d}t}\omega_m = t_{em} - t_L \,, \tag{5}$$

- electromagnetic torque:

$$t_{em} = \mathrm{Im}\left(\boldsymbol{\Psi}_s^* \mathbf{i}_s\right), \tag{6}$$

where $\mathbf{u}_s$ – stator voltage vector, $\mathbf{i}_s$, $\mathbf{i}_r$, – stator and rotor current vectors, $\boldsymbol{\Psi}_s$, $\boldsymbol{\Psi}_r$ – stator and rotor flux vectors, respectively, ω_m – rotor speed, r_s, r_r – stator and rotor resistances, l_s, l_r, l_m – stator, rotor and magnetizing inductances, respectively, $l_r = l_{\sigma r} + l_m$, $l_s = l_{\sigma s} + l_m$, t_L – load torque, T_M – mechanical time constant of the drive, $T_N = 1/(2\pi f_{sN})$ – time constant resulting from [p.u.] system.

2.2. DTC–SVM scheme

Direct torque control is one of the most popular vector control methods, firstly published by Depenbrock [41] and by Takahasi and Noguchi [42]. According to the DTC idea, the electromagnetic torque can be controlled by the amplitudes of the rotor and stator fluxes, and the angle, δ_Ψ, between them:

$$t_{em} = \frac{l_m}{l_s l_r - l_m^2} \Psi_r \Psi_s \sin\delta_\Psi \,, \tag{7}$$

where Ψ_r, Ψ_s are the amplitudes of the rotor and stator flux vectors.

Vectors of the stator and rotor fluxes are connected to each other in accordance with:

$$\boldsymbol{\Psi}_s = \frac{l_m}{l_r}\boldsymbol{\Psi}_r + \frac{l_s l_r - l_m^2}{l_r}\mathbf{i}_s \,. \tag{8}$$

Because the stator winding time constant is lower than the rotor time constant, fast changes of stator voltage cause an immediate change in the position of the stator flux vector and consequently in the angle between the stator and rotor flux vectors, resulting in a very fast and direct change of the IM electromagnetic torque. Over the years, a simple hysteresis control of the stator flux and electromagnetic torque and the control solution based on the switching table (DTC–ST) was substituted by the space vector modulation (SVM) with PI controllers [43]. This well-known scheme of the DTC–SVM structure is presented in Fig. 1.

The calculated electromagnetic torque, t_{em}, is compared with the reference torque, t_{em}^{ref}, from the speed regulator output (PI regulator in the structure under test). The torque error signal is sent to the PI controller of the u_{sy}^{ref} component of the stator voltage vector, which for the stabilized stator flux directly controls the motor torque, according to the well-known relationship [43]:

$$t_{em} = \frac{1}{r_s}\Psi_s u_{sy} \,. \tag{9}$$

In the second path of stator flux control, its set constant value is compared with the actual value determined by the flux estimator. In the case of this work, in the postfault operation of the drive system, the stator flux is calculated indirectly by the estimator of the stator current and rotor flux vector components (VCS), based on the relationship in equation (8). The flux error signal is fed to the PI regulator of the second component of the stator voltage vector, u_{sx}^{ref}. Then, the components of the voltage vector in the rotating coordinate system $(x-y)$ are transformed to the stationary system $(\alpha-\beta)$ and constitute the inputs to the SVM modulator block, forming the logic signals S_{ABC} for the VSI transistors.

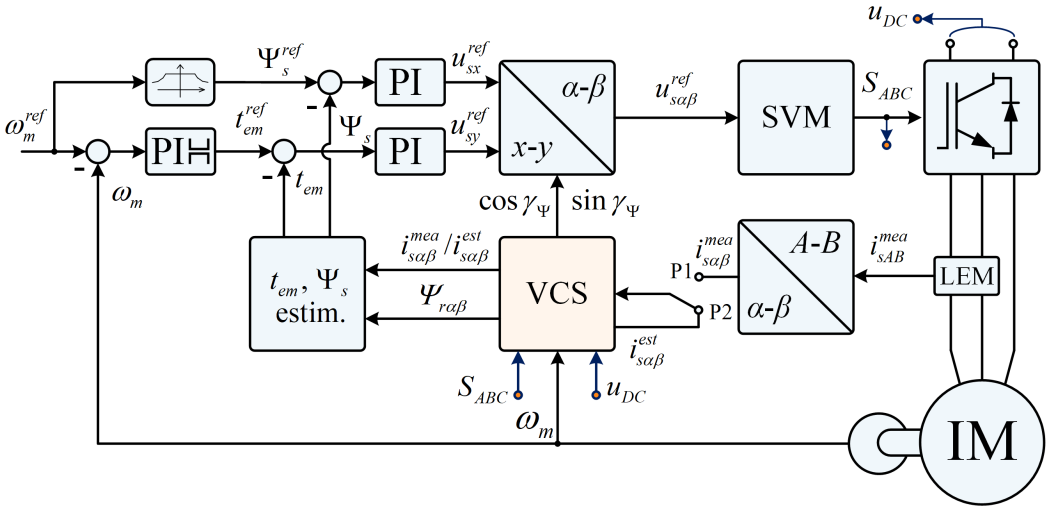

Fig. 1. Scheme of the DTC–SVM structure for induction motor

Under normal operation of the drive system, when all stator CSs are healthy, the stator flux and motor torque estimation for the DTC–SVM control structure is based on the measured stator currents in phases A and B (switch P in position P1 in Fig. 1) and rotor flux components calculated by VCS. When one or two CSs are damaged, the stator currents are estimated using VCS (switch P in position P2 in Fig. 1).

Although this structure does not include stator current regulators, unlike the FOC, information about the stator current is necessary to calculate the actual values of the IM stator flux and the electromagnetic torque. Therefore, the failures of stator current sensors are crucial for the DTC–SVM operation, and therefore suitable methods of the stator current reconstruction must be used in the postfault operation of the drive.

3. STATOR CURRENT RECONSTRUCTION FOR FAULT-TOLERANT CONTROL

The stator current reconstruction in the postfault operation of the drive system is realized in this work using the VCS algorithm for estimating the stator current, presented in detail in [31]. It consists of three systems of equations, the current model of the rotor flux equation (10), the stator current estimator equation (11), and the stator voltage estimator equation (12a), (12b) for simulation and equation (12c), (12d) for experimental tests, presented in a stationary reference frame:

$$T_N \frac{\mathrm{d}}{\mathrm{d}t}\Psi^i_{r\alpha} = \frac{r_r}{l_r}\left(l_m i^{est}_{s\alpha} - \Psi^i_{r\alpha}\right) - \omega_m \Psi^i_{r\beta}, \tag{10a}$$

$$T_N \frac{\mathrm{d}}{\mathrm{d}t}\Psi^i_{r\beta} = \frac{r_r}{l_r}\left(l_m i^{est}_{s\beta} - \Psi^i_{r\beta}\right) + \omega_m \Psi^i_{r\alpha}, \tag{10b}$$

$$T_N \frac{\mathrm{d}}{\mathrm{d}t} i^{est}_{s\alpha} = \frac{1}{l_s\sigma}\left(u_{s\alpha} - r_s i^{est}_{s\alpha} - T_N \frac{l_m}{l_r}\frac{\mathrm{d}}{\mathrm{d}t}\Psi^i_{r\alpha}\right), \tag{11a}$$

$$T_N \frac{\mathrm{d}}{\mathrm{d}t} i^{est}_{s\beta} = \frac{1}{l_s\sigma}\left(u_{s\beta} - r_s i^{est}_{s\beta} - T_N \frac{l_m}{l_r}\frac{\mathrm{d}}{\mathrm{d}t}\Psi^i_{r\beta}\right), \tag{11b}$$

$$u_{s\alpha} = \frac{1}{3}\left(2S_A - S_B - S_C\right)u_{DC}, \tag{12a}$$

$$u_{s\beta} = \frac{\sqrt{3}}{3}\left(S_B - S_C\right)u_{DC}, \tag{12b}$$

$$u_{s\alpha} = \frac{1}{3}\left(2d_A - d_B - d_C\right)u_{DC}, \tag{12c}$$

$$u_{s\beta} = \frac{\sqrt{3}}{3}\left(d_B - d_C\right)u_{DC}, \tag{12d}$$

where d_A, d_B, d_C – duty cycles from the SVM outputs.

To estimate these state variables using VCS only the DC voltage u_{DC} (in the DC-link of VSI) and the rotor angular velocity ω_m measurement are required.

The stator flux vector components and electromagnetic torque are calculated using equations (8) and (7), based on the components of stator current and rotor flux vectors estimated by VCS:

$$\Psi_{s\alpha\beta} = \frac{l_m}{l_r}\Psi^i_{r\alpha\beta} + \frac{l_s l_r - l_m^2}{l_r} i_{s\alpha\beta}, \tag{13}$$

$$t_{em} = \Psi_{s\alpha} i_{s\beta} - \Psi_{s\beta} i_{s\alpha}, \tag{14}$$

$$\Psi_s = \sqrt{\left(\Psi_{s\alpha}\right)^2 + \left(\Psi_{s\beta}\right)^2}, \tag{15}$$

with stator flux angle necessary for axes transformation from rotating to a stationary reference frame:

$$\sin\gamma_\Psi = \frac{\Psi_{s\beta}}{\Psi_s}, \qquad \cos\gamma_\Psi = \frac{\Psi_{s\alpha}}{\Psi_s}. \tag{16}$$

4. ANALYSIS OF THE STATOR AND ROTOR RESISTANCE INFLUENCE TO THE STATOR CURRENT RECONSTRUCTION IN DTC–SVM STRUCTURE

Simulation tests were conducted in the MATLAB/Simulink environment, using the Euler integration method (ode1), with sampling time $T_s = 6.25\mathrm{e}-6$, for the IM parameters given in the Appendix. It is well known that stator flux calculation is sensitive to stator and rotor resistance, depending on the direct or indirect method used. In the fault-free operation, to avoid problems with the pure integration of the direct method, the indirect calculation of the stator flux components based on the rotor flux and stator current should be used, as shown in Section 3. In a postfault operation, it does not matter which estimator will be used because their responses are identical when the stator current estimated by VCS is used.

The VCS algorithm is most susceptible to changes in rotor resistance, while in the DTC structure, the stator flux must be estimated, which in turn depends on the stator resistance. Therefore, the influence of changes in these two parameters on the quality of the drive system operation was tested, for 50% of the rated load and different angular velocities in the range from 10% to 100% of the rated value. Due to the three-phase symmetry of the IM, only currents estimated (*est*) and measured (*mea*) in phase A are presented in the following figures under stator and rotor resistance changed in the IM mathematical model. The currents transients are presented for linear change of the speed reference to an assumed value, ω_m^{ref}, next close to $t = 2$ s the load torque was applied, and next, between $t = 3$ s and $t = 5$ s the slow reverse to the opposite speed reference, ω_m^{ref}, was realized as presented in Fig. 2.

First, the influence of the increase in the rotor resistance up to 125% of its rated value was assumed and results are presented in Fig. 2(a, c, e, g).

As can be seen, despite the increase in the value of the rotor resistance by 25%, the character of the estimated current is correct. There are only slight differences in the amplitudes between the measured and estimated variables. For approximately t = 2.5 s, the absolute values of these differences expressed in [p.u.] are: 0.0932 (a), 0.0913 (c), 0.0830 (e) and 0.0598 (g), for the respective reference speed values.

Next, similar tests were conducted for the changed stator resistance in the IM model. The results of the estimated and measured currents in phase A are shown in Fig. 2(b, d, f, h).

From the obtained transients it can be seen that the change of stator resistance has a negligible influence on the estimated stator current. The greatest differences in amplitudes between

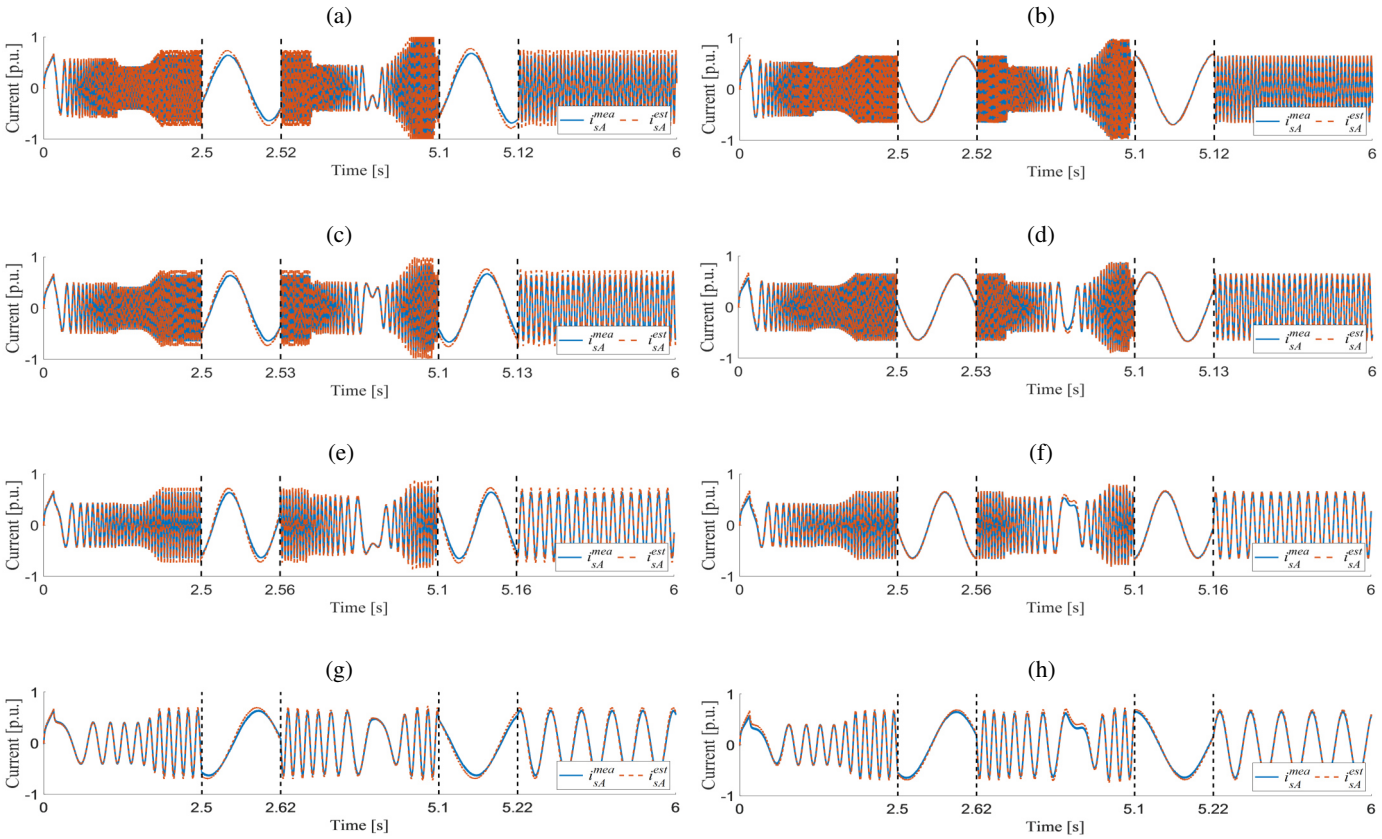

Fig. 2. Waveforms of the measured and estimated stator current in phase A for $\omega_m^{ref} = \pm\omega_{mN}$ (a, b), $\omega_m^{ref} = \pm 0.7\omega_{mN}$ (c, d), $\omega_m^{ref} = \pm 0.4\omega_{mN}$ (e, f), $\omega_m^{ref} = \pm 0.1\omega_{mN}$ (g, h), $r_r^{IM} = 1.25 r_{rN}$, $r_s^{IM} = r_{sN}$ (a, c, e, g) and $r_r^{IM} = r_{rN}$, $r_s^{IM} = 1.25 r_{sN}$ (b, d, f, h)

measured and estimated currents are seen for low motor speeds. Similarly to the previous analysis, for $t = 2.5$ s, the differences in amplitudes are: 0.0044 (b), 0.0065 (d), 0.0119 (f), 0.0391 (h), for the respective rotor reference speeds.

5. SIMULATION AND EXPERIMENTAL TESTS

5.1. Simulation assumptions

The parameters and the simulation environment are presented in Section 4. To reproduce the results of the simulation tests more accurately, some measurement noises were added:

- measuring noise in the stator current and DC voltage of VSI approximately ±0.01 [p.u.],
- an error in counting encoder pulses, depending on the current angular velocity.

The ideal (*id*) and measured (*mea*) variables are shown in Fig. 3.

5.2. Description of the experimental setup and test scenario

The experimental tests were realized using the laboratory setup (Fig. 4), consisting of two coupled IMs (1.1 kW – driving motor and 1.5 kW – loading motor), powered by two VSIs. The dSpace 1103 was used for rapid prototyping of the control structure. LEM type transducers were used for current measurements in phase A and phase B, while the speed was measured with an encoder (5000 imp/rev). The control signals for both VSIs were transmitted by the fiber-optics card, while the switching frequency of VSI was 8 kHz. Rated parameters of IM, controlled in the DTC–SVM structure have been presented in Table 1 in the Appendix.

Firstly, the quality of the stator current estimation for different working conditions was studied. Next, the tests scenario included different operating conditions of the DTC–SVM drive

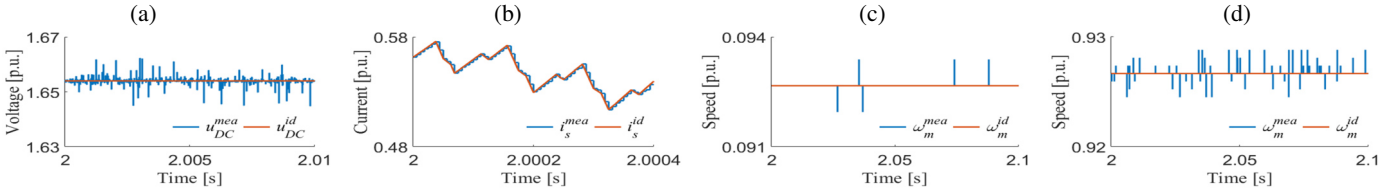

Fig. 3. Influence of measurement errors on selected signals in the drive system: DC voltage (a), stator current (b), low (c), and nominal rotor speed (d)

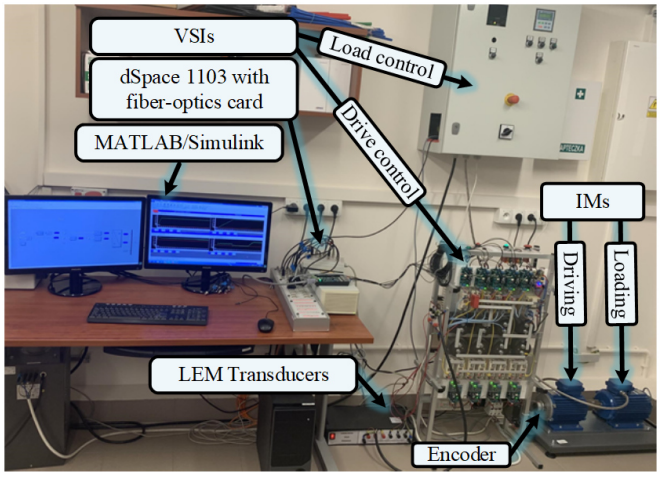

Fig. 4. The photo with the structure of the laboratory setup

system after a complete outage of both CSs, with stator currents reconstructed using VCS:

- slow start-up, regenerative brake, and slow reversal operation under regenerating mode with 50% of the rated load torque,
- operation at the rated speed under changeable load torque.

All tests for the above two points were carried out in the CSs postfault mode, and the stator currents were measured in experimental tests only for comparison purposes.

5.3. Quality of the stator current estimation for different operating conditions of the experimental drive

In this experimental test, the drive system used measured stator currents in different operating conditions, while the estimated stator currents estimated using VCS were compared to determine its estimation quality.

The tests were performed in a steady-state for different reference speeds, ω_m^{ref}, in the wide range of $\{0.05, 0.1, 0.15, 0.2, 0.25, 0.3, 0.4, 0.5, 0.6, 0.8, 1\}\omega_{mN}$ and two values of the load torque in motoring and regenerating modes and under non-load condition $\{-1, 0.5, 0, 0.5, 1\}t_{LN}$. To determine these errors the RMSE values for α and β components of the stator current were calculated in a time range equal to 2 s (from t_1 to t_2) and next the stator current estimation index is proposed as an average of α and β RMSEs values:

$$\Delta i_{sp} = \sqrt{\frac{\sum_{k=t_1/T_s}^{t_2/T_s} \left(i_{sp}^{mea}(k) - i_{sp}^{est}(k)\right)^2}{(t_2 - t_1)/T_s + 1}}, \quad p \in \{\alpha, \beta\}, \tag{17}$$

$$\Delta i_s = \frac{\Delta i_{s\alpha} + \Delta i_{s\beta}}{2}. \tag{18}$$

Received relative current estimation index values are shown in Fig. 5, while their detailed numbers are presented in Table A2. As can be seen, the best quality of stator current estimation is obtained for motoring mode or non-load system. In the regenerating mode, a bigger error can be observed, especially for low speeds. However, it should be noted that IM drives are designed to work close to rated values, and the proposed solution is primarily intended to ensure safe and stable postfault operation, until the defective CSs will be repaired.

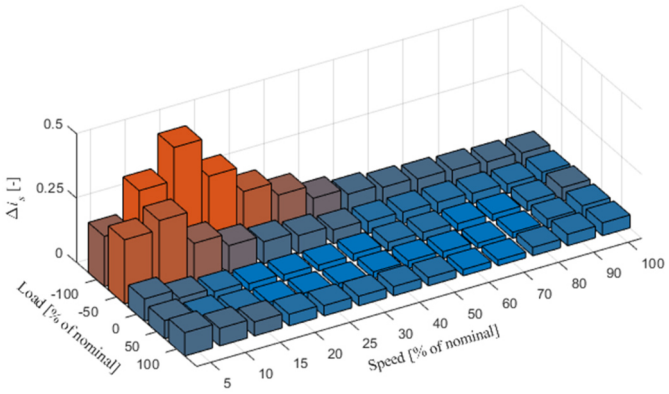

Fig. 5. RMSE values of stator current estimation index for different load torque and speed values

5.4. Postfault operation at different operating conditions

In these tests, the DTC drive operated with VCS in the postfault operation, while the real stator currents were measured only for comparison. Presented tests were conducted for different reference speeds in the range of $\{0.05, 0.4, 0.7\}\omega_{mN}$, under start-up, regenerative braking, and reversal operation under regenerative load torque. The IM was excited first at $t = 0$ s, and the rotor speed was activated when the reference value of the stator flux, given over the ramp reached the nominal value (≈ 0.16 s).

For all three different reference speeds, the start of the IM lasted 1 s. Next, in $t = 1.5$ s a constant load torque (50% of the rated value) was applied. In $t = 4.5$ s the direction of the load torque was changed (regenerative braking), and in $t = 7.5$ s the speed was reversed, under regenerative load torque.

The waveforms of the angular speeds, torques, and currents in phase A, for simulation (a, c, e) and experimental (b, d, f) tests are shown in Fig. 6 for 70% of rated speed, Fig. 7 for 40% of rated speed and Fig. 8 for 5% of rated speed. Because the waveform of the stator flux magnitude (Ψ_s) is almost identical, it was presented only for 70% of the rated speed (Fig. 6g,h).

The presented simulation studies together with their experimental verification demonstrate the high efficiency of the VCS algorithm in the DTC–SVM structure. As can be seen on the waveforms in Fig. 6g,h the stator flux is properly stabilized. In each tested case the measured speed with high accuracy tracks the reference speed (Figs. 6–8a,b). The electromagnetic torque coincides with the reference load value generated using an inverter supplying the loading IM (Fig. 4), for experimental tests presented in Figs. 6–8c,d, respectively. In steady states, it exhibits small oscillations, which are especially noticeable in the case of very low angular velocities (Fig. 8d). However, this does not significantly affect the quality of the drive system operation. The stator current in phase A is estimated correctly as presented in Figs. 6–8e,f, also when the system is operating in the very low-speed range in the real drive system (Fig. 8f). The stator current estimation is better for the motoring mode, and a little

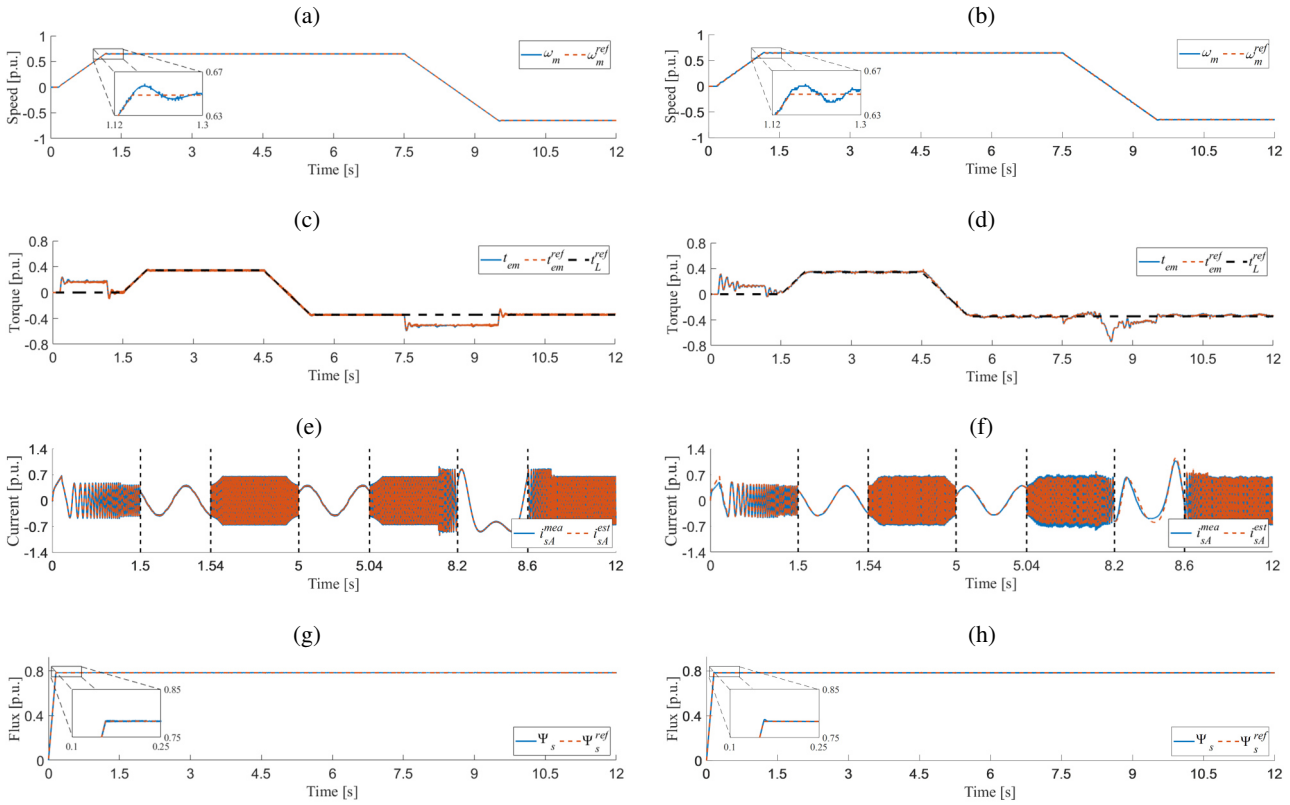

Fig. 6. Waveforms of the drive state variables under start-up, regenerative braking and slow reverse for $\omega_m^{ref} = \pm 0.7\omega_{mN}$, under motoring and regenerating modes; reference and actual motor speeds (a, b), reference and actual torques (c, d), measured and estimated stator currents in phase A (e, f); reference and actual stator fluxes (g, h); simulation (a, c, e, g) and experimental (b, d, f, h) test results

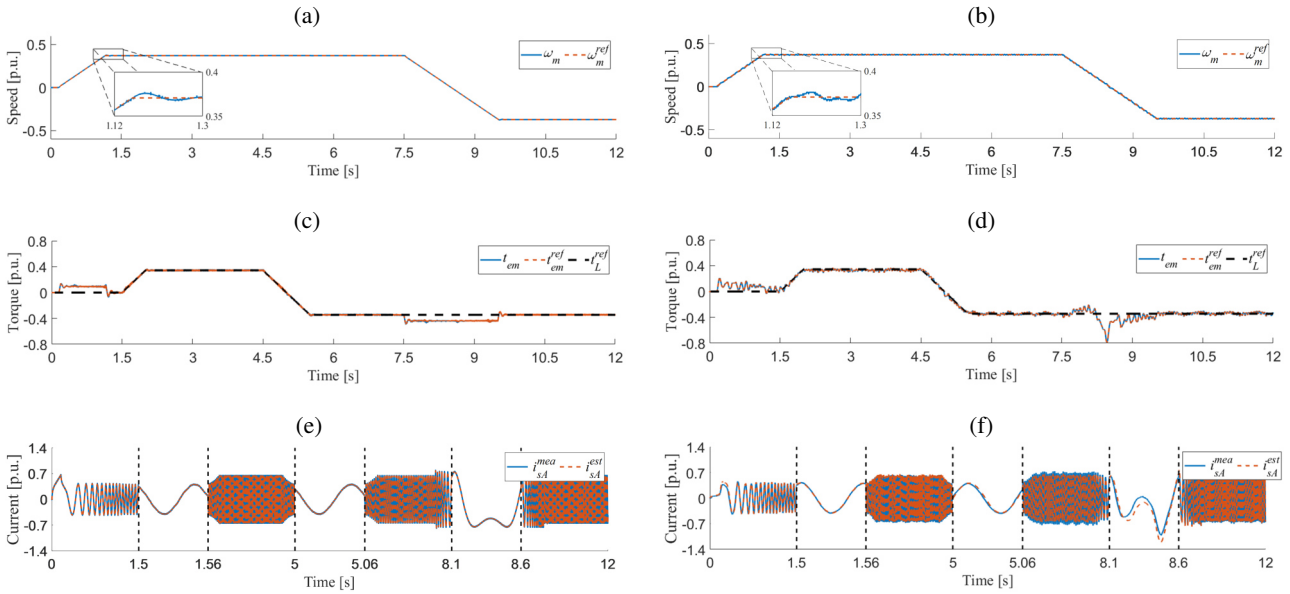

Fig. 7. Waveforms of the drive state variables under start-up, regenerative braking and slow reverse for $\omega_m^{ref} = \pm 0.4\omega_{mN}$, under motoring and regenerating modes; reference and actual motor speeds (a, b), reference and actual torques (c, d), measured and estimated stator currents in phase A (e, f); simulation (a, c, e) and experimental (b, d, f) test results

worse for the regenerating mode. The biggest error of the stator current estimation can be seen during the speed reverse when its value is close to zero.

The greatest estimation errors visible under the experimental test are caused by changes of the IM parameters with changeable operating points of the drive system, especially for very

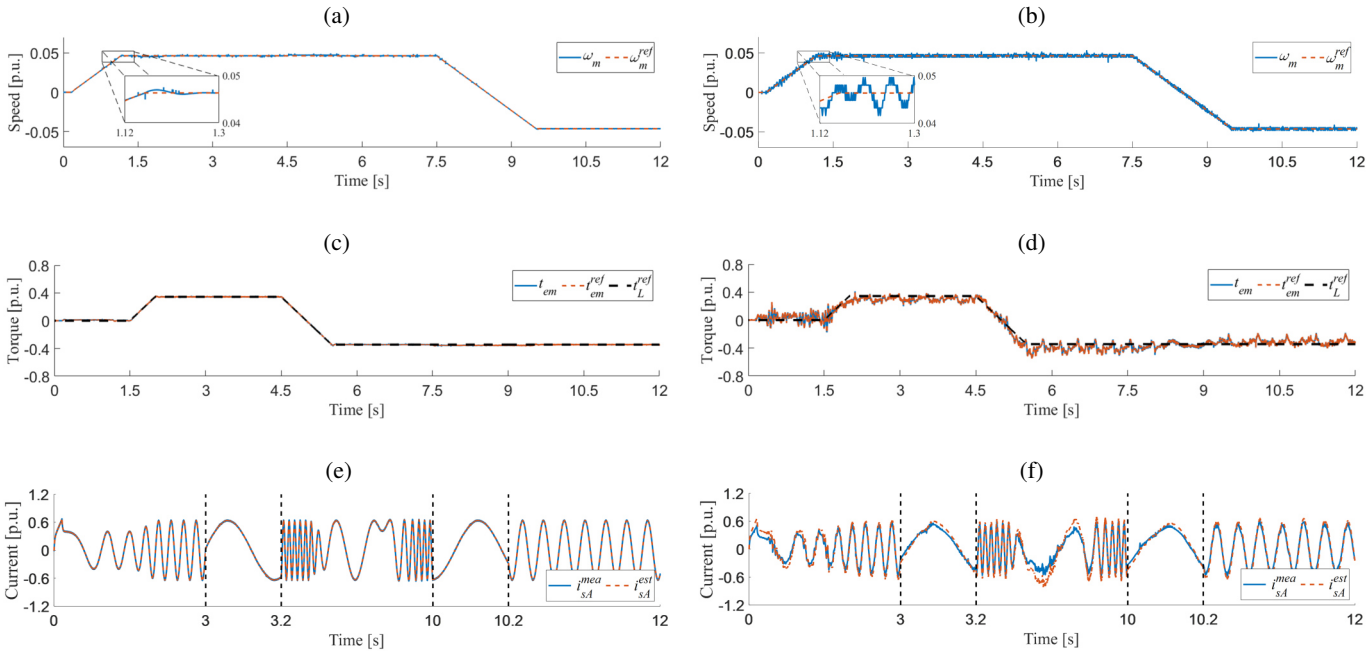

Fig. 8. Waveforms of the drive state variables under start-up, regenerative braking and slow reverse for $\omega_m^{ref} = \pm 0.05\omega_{mN}$, under motoring and regenerating modes; reference and actual motor speeds (a, b), reference and actual torques (c, d), measured and estimated stator currents in phase A (e, f); simulation (a, c, e) and experimental (b, d, f) test results

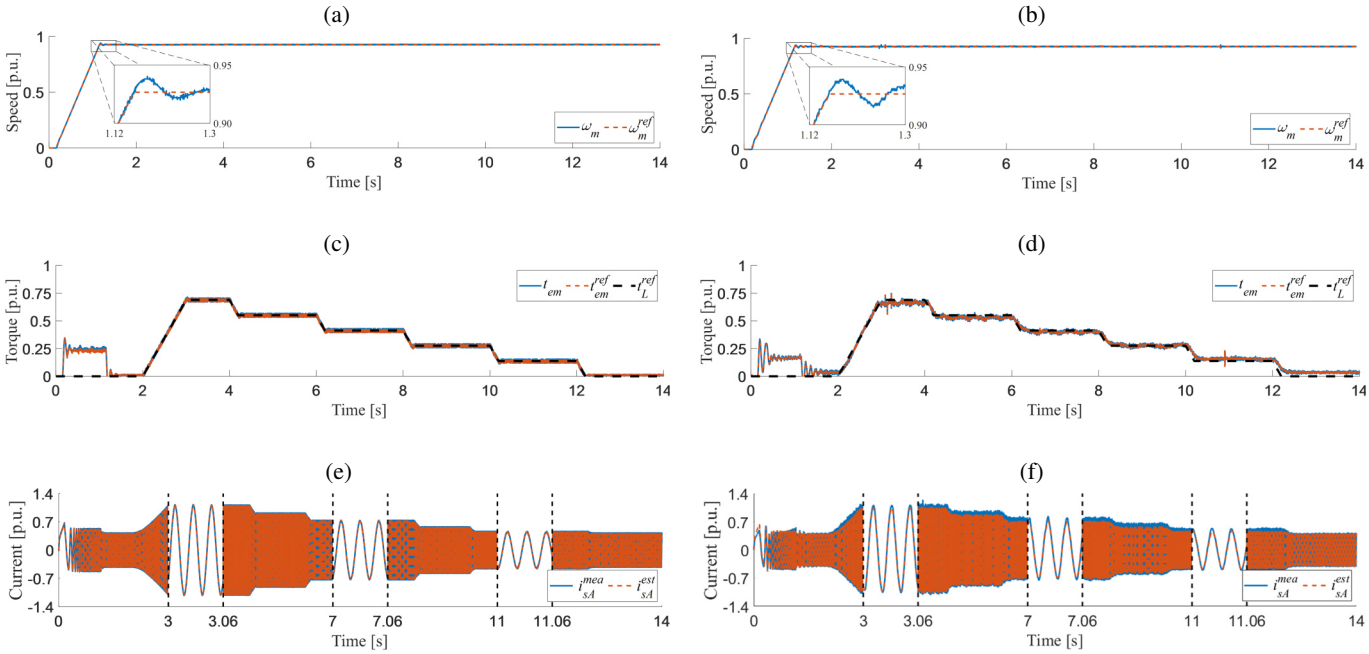

Fig. 9. Waveforms of the drive state variables under step changes of the load torque; $\omega_m^{ref} = \omega_{mN}$: reference and actual motor speeds (a, b), reference and actual torques (c, d), stator currents in phase A (e, f); simulation (a, c, e) and experimental (b, d, f) test results

low reference speed (close to zero) and under regenerating mode (Fig. 8d). To show better the estimation accuracy obtained by VSC including IM parameter changes in the experimental test, the stator current amplitudes are shown for all analysed cases (Figs. 6–9) and are presented in Fig. 10a–c. Next, the behavior of the drive system without measured stator currents was tested for constant, rated speed and different load torque values in the range of $\{0, 0.2, 0.4, 0.6, 0.8, 1\}t_{LN}$. Simulation (a) and experimental (b) test results for reference and actual torques and speeds are presented in Fig. 9.

It can be seen from the presented tests that the torque control is properly realized based on the estimated stator currents after the failure of all CSs in the drive system. The electromagnetic torque of the IM is correctly estimated and stabilized (see

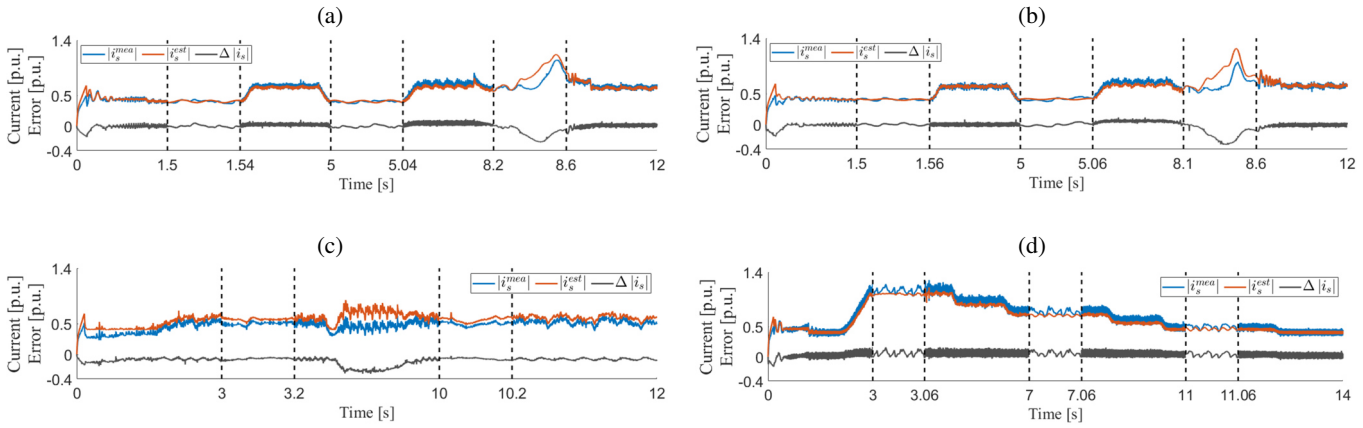

Fig. 10. Waveforms of the measured and estimated stator current amplitudes for $t_L = \pm 0.5 t_{LN}$ and: $\omega_m^{ref} = \pm 0.7 \omega_{mN}$ (a), $\omega_m^{ref} = \pm 0.4 \omega_{mN}$ (b), $\omega_m^{ref} = \pm 0.05 \omega_{mN}$ (c) and for $t_L = \{0, 0.2, 0.4, 0.6, 0.8, 1\} t_{LN}$, $\omega_m^{ref} = \omega_{mN}$ (d)

Fig. 9c,d) using estimated components of the stator current vector and next, the components of flux vector required by the control structure in the studied range of load torque changes. The angular velocity is properly stabilized (Fig. 9a,b) whereas stator currents are estimated with good accuracy (Fig. 9e,f). It can be seen in Fig. 10d that the amplitude of estimated stator current is characterized by a smaller noise than amplitude of measured current, which is caused by a lack of measuring noise.

6. CONCLUSIONS

The analysis of the above results allows us to conclude that the use of the VCS algorithm in the DTC–SVM control structure of IM drive without stator current measurement is very effective and can be applied in the CS–FTC system. In addition, numerous experiments have shown excellent dynamic properties of the control system, a very good stator current reconstruction in the steady-states and satisfactory quality of current estimation under transients. It should be highlighted that the proposed control structure works correctly throughout the studied scenarios and different operating conditions of the drive system. Although the stator current reconstruction is quite good under steady-state operation in experimental tests, the estimation errors occurring under reverse close to zero speed and in regenerating mode should be further studied and some parameter estimation procedures should be included in the future research to obtain higher current estimation quality in this operating range.

However, taking into account the fact that after detecting all current sensors damage, the drive should operate in the postfault mode only for a limited period, the obtained stator current reconstruction quality ensures correct operation of the algorithms for estimating the amplitude and position of the stator flux vector and the electromagnetic torque of the motor, and thus correct operation of the DTC–SVM drive system. It is shown that in all mentioned operating points the DTC–SVM IM drive operates properly without stator current measurement, thus this solution can be adapted in drives dedicated to systems with higher safety level requirements, like, e.g. electric vehicle drives (EVD).

APPENDIX

Table 1
Rated parameters of IM

Symbol	[ph.u.]	[p.u.]
Rated phase voltage, U_N	230 V	0.707
Rated phase current, I_N	2.5 A	0.707
Rated power, P_N	1.1 kW	0.638
Rated speed, n_N	1390 rpm	0.927
Rated torque, T_{eN}	7.56 Nm	0.688
Number of pole pairs, p_b	2	–
Rotor winding resistance, R_r	4.968 Ω	0.0540
Stator winding resistance, R_s	5.114 Ω	0.0556
Rotor leakage inductance, $L_{\sigma r}$	31.6 mH	0.1079
Stator leakage inductance, $L_{\sigma s}$	31.6 mH	0.1079
Main inductance, L_m	541.7 mH	1.8498
Rated rotor flux, Ψ_{rN}	0.7441 Wb	0.7187
Rated stator flux, Ψ_{sN}	0.8235 Wb	0.7954
Rated magnetic flux, Ψ_{mN}	0.7518 Wb	0.7261
Mechanical time constant, T_M	0.25 s	–

Table 2
Values of the stator current estimation error index Δi_s

$\omega_m \setminus t_L$	–100%	–50%	0%	50%	100%
5%	0.1950	0.2489	0.0868	0.0700	0.0905
10%	0.3336	0.2846	0.0513	0.0462	0.0684
15%	0.4622	0.1574	0.0375	0.0326	0.0543
20%	0.3116	0.1096	0.0290	0.0245	0.0452
25%	0.2133	0.0854	0.0250	0.0209	0.0397
30%	0.1606	0.0704	0.0231	0.0200	0.0374
40%	0.1091	0.0540	0.0279	0.0258	0.0359
50%	0.0860	0.0475	0.0339	0.0295	0.0322
60%	0.0738	0.0456	0.0339	0.0263	0.0242
80%	0.0673	0.0440	0.0289	0.0204	0.0223
100%	0.0622	0.0401	0.0262	0.0237	0.0325

REFERENCES

[1] M.O. Mustafa, G. Nikolakopoulos, and T. Gustafsson, "Faults Classification Scheme for Three Phase Induction Motor", *Int. J. Syst. Dyn. Appl.*, vol. 3, no. 1, pp. 1–20, 2014, doi: 10.4018/ijsda.2014010101.

[2] R. Peuget, S. Courtine, and J.P. Rognon, "Fault detection and isolation on a pwm inverter by knowledge-based model", *IEEE Trans. Ind. Appl.*, vol. 34, no. 6, pp. 1318–1326, 1998, doi: 10.1109/28.739017.

[3] A. Gaeta, G. Scarcella, G. Scelba, S. De Caro, and A. Testa, "Inverter fault-identification for VSI motor drives", in *8th IEEE Symp. Diagnostics Electr. Mach. Power Electron. Drives (SDEMPED)*, 2011 pp. 413–419, doi: 10.1109/DEMPED.2011.6063656.

[4] M.D. Kumar, "Fault Analysis For Voltage Source Inverter Driven Induction Motor Drive", *Int. J. Electr. Eng. Technol.*, vol. 8, no. 1, pp. 1–8, 2017.

[5] T. Orlowska-Kowalska and P. Sobanski, "Simple diagnostic technique of a single IGBT open-circuit faults for a SVM-VSI vector controlled induction motor drive", *Bull. Polish Acad. Sci. Tech. Sci.*, vol. 63, no. 1, pp. 281–288, 2015, doi: 10.1515/bpasts-2015-0032.

[6] M. Trabelsi, M. Boussak, and M. Gossa, "Multiple IGBTs open circuit faults diagnosis in voltage source inverter fed induction motor using modified slope method", in *19th Int. Conf. Electr. Mach. (ICEM)* 2010, pp. 1–6, doi: 10.1109/ICELMACH.2010.5608044.

[7] K. Rothenhagen and F.W. Fuchs, "Model-based fault detection of gain and offset faults in doubly fed induction generators", in *2009 IEEE Int. Symp. Diagnostics Electr. Mach. Power Electron. Drives (SDEMPED)*, 2009, pp. 1–6, doi: 10.1109/DEMPED.2009.5292752.

[8] H. Berriri, M.W. Naouar, and I. Slama-Belkhodja, "Parity space approach for current sensor fault detection and isolation in electrical systems", in *Int. Multi-Conference Syst. Signals Devices (SSD) – Summ. Proc.*, 2011, pp. 0–6, doi: 10.1109/SSD.2011.5767496.

[9] A. Akrad, M. Hilairet, and D. Diallo, "Design of a fault-tolerant controller based on observers for a PMSM drive", *IEEE Trans. Ind. Electron.*, vol. 58, no. 4, pp. 1416–1427, 2011, doi: 10.1109/TIE.2010.2050756.

[10] A. Ben Youssef, S.K. El Khil, and I. Slama-Belkhodja, "State observer-based sensor fault detection and isolation, and fault tolerant control of a single-phase PWM rectifier for electric railway traction", *IEEE Trans. Power Electron.*, vol. 28, no. 12, pp. 5842–5853, 2013, doi: 10.1109/ TPEL.2013.2257862.

[11] H. Berriri, M.W. Naouar, and I. Slama-Belkhodja, "Easy and fast sensor fault detection and isolation algorithm for electrical drives", *IEEE Trans. Power Electron.*, vol. 27, no. 2, pp. 490–499, 2012, doi: 10.1109/ TPEL.2011.2140333.

[12] K.C. Kim, S.J. Hwang, K.Y. Sung, and Y.S. Kim, "A study on the fault diagnosis analysis of variable reluctance resolver for electric vehicle", in *Proc. IEEE Sensors*, 2010 pp. 290–295, doi: 10.1109/ICSENS.2010.5689869.

[13] F. Zidani, M.E.H. Benbouzid, D. Diallo, and A. Benchaïb, "Active fault-tolerant control of induction motor drives in EV and HEV against sensor failures using a fuzzy decision system", in *IEEE Int. Electr. Mach. Drives Conf. (IEMDC)*, 2003, vol. 2, pp. 677–683, doi: 10.1109/IEMDC.2003.1210309.

[14] T.A. Najafabadi, F.R. Salmasi, and P. Jabehdar-Maralani, "Detection and isolation of speed-, DC-link voltage-, and current-sensor faults based on an adaptive observer in induction-motor drives", *IEEE Trans. Ind. Electron.*, vol. 58, no. 5, pp. 1662–1672, 2011, doi: 10.1109/TIE.2010.2055775.

[15] S. Fan and J. Zou, "Sensor Fault detection and fault tolerant control of induction motor drivers for electric vehicles", in Conf. Proc. *IEEE 7th Int. Power Electron. Motion Control Conf. (IPEMC)*, 2012, vol. 2, pp. 1306–1309, doi: 10.1109/IPEMC.2012.6259046.

[16] M. Bouakoura, N. Naăźt-Saăźd, and M.-S. Naăźt-Saăźd, "Speed Sensor Faults Diagnosis in an Induction Motor Vector Controlled Drive", *Acta Electrotech. Inform.*, vol. 17, no. 1, pp. 49–51, 2017, doi: 10.15546/aeei-2017-0007.

[17] K. Klimkowski and M. Dybkowski, "A comparative analysis of the chosen speed sensor faults detectors for induction motor drives", in *Int. Conf. Electr. Drives Power Electron. (EDPE)*, 2015, pp. 333–338, doi: 10.1109/EDPE.2015.7325316.

[18] F.R. Salmasi and T.A. Najafabadi, "An adaptive observer with online rotor and stator resistance estimation for induction motors with one phase current sensor", *IEEE Trans. Energy Convers.*, vol. 26, no. 3, pp. 959–966, 2011, doi: 10.1109/TEC.2011.2159007.

[19] Z. Gao, C. Cecati, and S.X. Ding, "A Survey of Fault Diagnosis and Fault-Tolerant Techniques – Part I: Fault Diagnosis With Model-Based and Signal-Based Approaches", *IEEE Trans. Ind. Electron.*, vol. 62, no. 6, pp. 3757–3767, Jun. 2015, doi: 10.1109/TIE.2015.2417501.

[20] Z. Gao, C. Cecati, and S. Ding, "A Survey of Fault Diagnosis and Fault-Tolerant Techniques – Part II: Fault Diagnosis with Knowledge-Based and Hybrid/Active Approaches", *IEEE Trans. Ind. Electron.*, vol. 62, no. 6, pp. 3768–3774, 2015, doi: 10.1109/TIE.2015.2419013.

[21] M. Dybkowski, K. Klimkowski, and T. Orłowska-Kowalska, "Speed and current sensor fault-tolerant-control of the induction motor drive", in *Stud. Syst. Decis. Control*, J. Kabzinski, Ed., Springer, Cham, 2017 vol. 75, pp. 141–167, doi: 10.1007/978-3-319-45735-2_7.

[22] T. Orłowska-Kowalska, C.T. Kowalski, and M. Dybkowski, "Fault-diagnosis and fault-tolerant-control in industrial processes and electrical drives", in *Stud. Syst. Decis. Control*, J. Kabzinski, Ed., Springer, Cham, 2017, vol. 75, pp. 101–120, doi: 10.1007/978-3-319-45735-2_5.

[23] Xiaodong Shi and M. Krishnamurthy, "Survivable Operation of Induction Machine Drives With Smooth Transition Strategy for EV Applications", *IEEE J. Emerg. Sel. Top. Power Electron.*, vol. 2, no. 3, pp. 609–617, 2014, doi: 10.1109/jestpe.2014.2303488.

[24] M. Manohar and S. Das, "Current Sensor Fault-Tolerant Control for Direct Torque Control of Induction Motor Drive Using Flux-Linkage Observer", *IEEE Trans. Ind. Informatics*, vol. 13, no. 6, pp. 2824–2833, 2017, doi: 10.1109/TII.2017.2714675.

[25] K.-S. Lee and J.-S. Ryu, "Instrument fault detection and compensation scheme for direct torque controlled induction motor drives", *IEE Proc. - Control Theory Appl.*, vol. 150, no. 4, pp. 376–382, 2003, doi: 10.1049/ip-cta:20030596.

[26] F.R. Salmasi, "A Self-Healing Induction Motor Drive With Model Free Sensor Tampering and Sensor Fault Detection, Isolation, and Compensation", *IEEE Trans. Ind. Electron.*, vol. 64, no. 8, pp. 6105–6115, 2017, doi: 10.1109/TIE.2017.2682035.

[27] F. Aguilera, P.M. de la Barrera, C.H. De Angelo, and D.R. Espinoza Trejo, "Current-sensor fault detection and isolation for induction-motor drives using a geometric approach", *Control Eng. Pract.*, vol. 53, pp. 35–46, 2016, doi: 10.1016/j.conengprac.2016.04.014.

[28] C. Chakraborty and V. Verma, "Speed and current sensor fault detection and isolation technique for induction motor drive using axes transformation", *IEEE Trans. Ind. Electron.*, vol. 62, no. 3, pp. 1943–1954, 2015, doi: 10.1109/TIE.2014.2345337.

[29] W. Wang, Y. Feng, Y. Shi, M. Cheng, W. Hua, and Z. Wang, "Fault-Tolerant Control of Primary Permanent-Magnet Linear Motors With Single Phase Current Sensor for Subway Applications", *IEEE Trans. Power Electron.*, vol. 34, no. 11, pp. 10546–10556, Nov. 2019, doi: 10.1109/TPEL.2019.2899168.

[30] Y. Yu, Y. Zhao, B. Wang, X. Huang, and D. Xu, "Current sensor fault diagnosis and tolerant control for VSI-based induction motor drives", *IEEE Trans. Power Electron.*, vol. 33, no. 5, pp. 4238–4248, 2018, doi: 10.1109/TPEL.2017.2713482.

[31] M. Adamczyk and T. Orlowska-Kowalska, "Virtual current sensor in the fault-tolerant field-oriented control structure of an induction motor drive", *Sensors (Switzerland)*, vol. 19, no. 22, 2019, doi: 10.3390/s19224979.

[32] Y. Azzoug, M. Sahraoui, R. Pusca, and T. Ameid, "High-performance vector control without AC phase current sensors for induction motor drives: Simulation and real-time implementation", *ISA Trans.*, vol. 109, pp. 295–306, 2021, doi: 10.1016/j.isatra.2020.09.021.

[33] M. Manohar and S. Das, "Notice of Removal: Current Sensor Fault-Tolerant Control of Induction Motor Driven Electric Vehicle Using Flux-Linkage Observer", in *2020 IEEE Transportation Electrification Conference & Expo (ITEC)*, 2020, pp. 884–889, doi: 10.1109/ITEC48692.2020.9161553.

[34] Y. Azzoug, R. Pusca, M. Sahraoui, A. Ammar, R. Romary, and A.J. Marques Cardoso, "A Single Observer for Currents Estimation in Sensor's Fault-Tolerant Control of Induction Motor Drives", in *2019 International Conference on Applied Automation and Industrial Diagnostics (ICAAID)*, 2019, pp. 1–6, doi: 10.1109/ICAAID.2019.8934969.

[35] W. Wang, M. Cheng, Z. Wang, and B. Zhang, "Fast switching direct torque control using a single DC-link current sensor", *J. Power Electron.*, vol. 12, no. 6, pp. 895–903, 2012, doi: 10.6113/JPE.2012.12.6.895.

[36] B. Metidji, N. Taib, L. Baghli, T. Rekioua, and S. Bacha, "Low-cost direct torque control algorithm for induction motor without AC phase current sensors", *IEEE Trans. Power Electron.*, vol. 27, no. 9, pp. 4132–4139, 2012, doi: 10.1109/TPEL.2012.2190101.

[37] H. Kim and T.M. Jahns, "Phase Current Reconstruction for AC Motor Drives using a DC-link Single Current Sensor and Measurement Voltage Vectors", in *IEEE 36th Conference on Power Electronics Specialists (PESC)*, 2006, pp. 1346–1352, doi: 10.1109/PESC.2005.1581804.

[38] Y. Xu, H. Yan, J. Zou, B. Wang, and Y. Li, "Zero Voltage Vector Sampling Method for PMSM Three-Phase Current Reconstruction Using Single Current Sensor", *IEEE Trans. Power Electron.*, vol. 32, no. 5, pp. 3797–3807, 2017, doi: 10.1109/TPEL.2016.2588141.

[39] M.P. Kazmierkowski, R. Krishnan, and F. Blaabjerg, *Control in Power Electronics – Selected Problems*, New York, USA: Academic, 2002.

[40] T. Orlowska-Kowalska, *Sensorless Induction Motor Drives*, Wrocław: Wroclaw University of Technology Press, 2003.

[41] M. Depenbrock, "Direct self-control (DSC) of inverter-fed induction machine", *IEEE Trans. Power Electron.*, vol. 3, no. 4, pp. 420–429, Oct. 1988, doi: 10.1109/63.17963.

[42] I. Takahashi and T. Noguchi, "A New Quick-Response and High-Efficiency Control Strategy of an Induction Motor", *IEEE Trans. Ind. Appl.*, vol. IA-22, no. 5, pp. 820–827, 1986, doi: 10.1109/TIA.1986.4504799.

[43] G.S. Buja and M.P. Kazmierkowski, "Direct Torque Control of PWM Inverter-Fed AC Motors – A Survey", *IEEE Trans. Ind. Electron.* vol. 51, no. 4, pp. 744–757, 2004, doi: 10.1109/TIE.2004.831717.